## PAPER

Check for updates

# Effect of a buffer/iodide electrolyte on the performance of electrochemical capacitors†

Amelia Klimek, [iD] Maciej Tobis [iD] and Elzbieta Frackowiak [iD] *

One of the major problems affecting the energetic characteristics and cycle life of electrochemical capacitors (ECs) utilizing aqueous electrolytes is the narrow operating voltage range, which is limited by the thermodynamic stability of water (1.23 V). An improvement in the EC energy can be realized by a capacitance and/or voltage increase. For that purpose, cost-effective and environmentally friendly iodides have been added to aqueous electrolytes to improve the redox activity. Moreover, buffer agents (acetate, citrate, and phosphate) that are well known for adjusting the pH of an electrolyte have been applied, which enabled ECs to reach a stable operating voltage of 1.5 V. After adding iodide to the buffer system, the conductivity increased notably, whereas the pH values remained nearly the same. Galvanostatic charge/discharge test (0.5 A g$^{-1}$) for ECs operating in buffer electrolytes containing 0.2 mol L$^{-1}$ NaI showed that this additive noticeably increased the specific capacitance values from 91 to 149 F g$^{-1}$ for acetate buffer, from 7 to 101 F g$^{-1}$ for citrate buffer, and from 22 to 132 F g$^{-1}$ for phosphate buffer. The long-time performance of the ECs was investigated through accelerated potentiostatic floating. The electrochemical performance was studied using various activated carbons. During the floating aging test, the YP50F-based EC working in acetate buffer with 0.2 mol L$^{-1}$ NaI displayed the best long-term performance (310 h) compared to YP80F and BP2000 carbons, which exhibited 212 h and 126 h, respectively. The highly microporous YP50F carbon in the acetate buffer/iodide electrolyte revealed the best wettability. Interestingly, the citrate buffer/iodide EC system with YP50F demonstrated an extremely long floating performance (1006 h). Thus, this study presents a new strategy for improving the energetic metrics and cycling performance of carbon-based ECs operating in buffer electrolytes with an iodide redox pair.

## 1. Introduction

The worldwide utilization of electrical energy is increasing rapidly owing to population growth and technological advancements. Currently, fossil fuels (*e.g.*, oil, coal, and natural gas) continue to be the base of global power systems, accounting for 64% of the world's electricity supply.[1] The main benefit of petroleum-based fuels is their incredible effectiveness. However, their major disadvantages are their limited resources in the earth's crust and the emission of $CO_2$ during their combustion, which contributes to the greenhouse effect. Consequently, natural and self-replenishing renewable energy sources are attracting increasing attention. However, these are often dependent on unstable weather conditions, such as the sun or wind. Additionally, the real-time operation of the power

grid presents an engineering problem since power is produced and consumed simultaneously, with generation fluctuating to maintain system balance.[1-3] To overcome this issue, various electrochemical storage systems, including batteries, redox flow batteries, and electrochemical capacitors (ECs), have been proposed. Batteries offer high energy density and a significant operating time; however, their use in several industries is limited by their low power density and poor cyclability. ECs, also known as supercapacitors, can overcome the drawbacks of batteries as they exhibit higher power densities, safety, green profile, and extended cycle life.[4] Consequently, ECs are widely used in various sectors, such as transportation,[5] aerospace,[6] medical devices,[7] construction, and building management.[8] ECs store energy through the formation of an electrical double-layer (EDL) at the electrode/electrolyte interface. Nonetheless, there is a possibility to increase the amount of stored energy thanks to fast faradaic reactions coming from *e.g.*, redox-active species.[9] There are several materials, such as graphene oxide,[10] activated carbon,[11] carbide derived carbon,[12] COF,[13] MOF,[14] MXenes,[15] and carbon nanotubes,[16] that can be utilized as electrode materials for ECs. Furthermore,

*Institute of Chemistry and Technical Electrochemistry, Poznan University of Technology, Berdychowo 4, Poznan 60-965, Poland.*
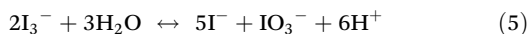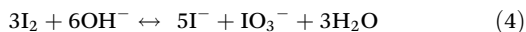*E-mail: elzbieta.frackowiak@put.poznan.pl*

†Electronic supplementary information (ESI) available. See DOI: https://doi.org/10.1039/d4gc01748j

the application of newly discovered quantum dots is attracting more and more interest.[17] Among the various carbon forms, activated carbon is the best due to its high surface area, low resistance, cost-effectiveness, high conductivity, chemical stability, and versality.[18] Electrolytes affect the characteristics of ECs, mostly the operating voltage window.[19] Typically, aqueous media,[20,21] organic media,[22] ionic liquids,[23] and deep eutectic solvents[24,25] can be utilized as EC electrolytes. An ideal EC electrolyte should be characterized by several parameters, such as cost-effectiveness, environmental friendliness, good conductivity, and wide operating voltage range, which should allow the EC to reach high energetic characteristics and long-term cycle life. In this sense, the aqueous-based electrochemical capacitor presents an excellent system, competitive to the organic one, that is also safe, green, and affordable.[26] Among the first water-based electrolytes utilized in ECs were KOH and $H_2SO_4$. However, such electrolytes cannot be considered for commercial application due to their narrow voltage window (ca. 0.8 V), limited by the thermodynamic stability of water[27] and corrosive character. Consequently, neutral solutions, such as sulfates ($Li_2SO_4$) and nitrates ($LiNO_3$), have been proposed, which can offer a higher voltage window up to 1.5 V by utilizing stainless steel current collectors. These neutral electrolytes enabled overcoming water splitting issues due to the electrosorption of hydrogen at the negative electrode.[28,29] Another approach is the use of buffer solutions as electrolytes in ECs. To date, there are a few papers that have reported the application of buffer solutions in ECs, but mainly as an additive to the neutral electrolyte.[30,31]

A weak or medium-strong acid/base and the equivalent salt are called buffers. When acids ($H^+$ ions) or bases ($OH^-$ ions) are introduced, a solution that functions as a buffer system resists to maintain the solution pH.[32] That is why buffers are mostly used for various experiments involving chemical/biological reactions,[33] calibration, and standardization to keep a stable pH environment.[34] Moreover, Salis et al. discovered an additional function of buffers in biological systems, in which buffers could compete for the adsorption at the charged surfaces with strong electrolytes, thus modulating the Hofmeister effect.[35] Regarding the application of buffers in energy-storage systems, Chien et al. discussed hydrogen adsorption/desorption in asymmetric activated carbon-based SCs, and proved that the additive of a buffer agent ($NaH_2PO_4$) into the neutral electrolyte ($Na_2SO_4$) could stabilize the local pH value at the electrode/electrolyte interface as weakly acidic, neutral, or weakly basic pH. They also showed it significantly increased the proton supply and the rate of hydrogen adsorption at the electrode/electrolyte interface, leading to a higher pseudocapacitive effect, in addition to changing the potential for hydrogen evolution.[30] Vindt et al. studied the effect of phosphate buffer ($K_2HPO_4$ + $KH_2PO_4$) in a neutral electrolyte ($KNO_3$) for carbon-based supercapacitors. The study confirmed that the wider operating voltage window of the EC based on the neutral electrolyte was mainly due to local pH changes at the electrode surface. Nevertheless, the buffer capacity, rather than the electrolyte's pH value, determined how strong the

effect was. By studying the impact of a buffer to neutral electrolytes, they demonstrated that a 56% higher storage capacity could be achieved by controlling the buffer capacity of the electrolyte.[31] In both cases, the experiments were done mostly using three-electrode cells utilizing mainly cyclic voltammetry.[30,31] Sodium acetate electrolytes, buffered by acetic acid, were used to alter the pH of the solution, and in turn to boost the pseudocapacitive behavior of supercapacitors utilizing MXenes as an electrode material,[36] and a molten-salt (MS) synthesis procedure of MXenes was proposed with the creation of –O and –Cl surface groups. The formation of such groups enabled a better compatibility with the acetate-based electrolytes. The authors reported achieving a high energy density (37 W h $kg^{-1}$) for an asymmetric supercapacitor based on MS-MXene as a negative electrode and $MnO_2$ as a positive electrode in 1 M sodium acetate (buffered at pH = 5). Moreover, the suppression of hydrogen evolution was observed.[36] Sugimoto et al. selected acetic acid-lithium acetate (AcOH-AcOLi) buffered solutions in various volume ratios as an electrolyte to study the origin and mechanism of the pseudocapacitance of ruthenium-based oxides in electrochemical capacitors.[37] The highest capacitance (1038 F $g^{-1}$) was obtained for $RuO_2$ nanosheet electrodes in 5 M AcOH-AcOLi (pH 5.4). They found that the pseudocapacitive behavior declined with lowering the pH when the volume ratio of AcOH-AcOLi was changed. While the extremely high capacitance values are promising; however, the use of ruthenium oxide in energy-storage devices is limited due to its high cost and toxicity.[37] Acetate salts (not necessarily in the form of a buffer) are becoming more popular today as aqueous electrolytes for high energy ECs due to their eco-friendliness, price, and high solubility in water. Piwek et al. studied carbon-based electrochemical capacitor operating in acetate-based salts, and reported that acetates ($Li^+$, $Na^+$, and $Mg^{2+}$) at molar concentrations ranging from 0.1 to 2 mol $L^{-1}$ with moderate conductivity values could have an impact on the maximum operating voltage and enable the EC voltage to be increased. An EC based on commercial YP50F carbon in 0.5 M $CH_3COONa$ reached 77 F $g^{-1}$ at 1.5 V (0.5 A $g^{-1}$). The aging of the same system was investigated by the floating method and displayed good capacitance retention after 130 h.[38] Potassium acetate due to its extremely high solubility in water was tested at various concentrations (20–60 wt%) by Matei Ghimbeu et al. An increase in the voltage window (1.8 V) and significantly improved capacitance (130 F $g^{-1}$ at 1 A $g^{-1}$) were achieved for a carbon-based EC operating in 40 wt% KOAc.[39] Despite enabling the significant extension of the operating voltage in neutral electrolytes, overcoming the thermodynamic stability of water, the systems lacked energy. An increase in capacitance and thus energy density of ECs could be achieved by the addition of redox-active species. Lota et al. reported a novel EC operating in 1 mol $L^{-1}$ potassium iodide for carbon-based ECs, which enabled double the capacitance values compared to ECs operating in 1 mol $L^{-1}$ $H_2SO_4$. The outstanding performance of the electrolyte only for the positive electrode was associated with the good conductivity and quick faradaic reac-

tions of the iodide. It is noteworthy that iodides are the most eco-friendly compared to the rest of the halides (*e.g.*, bromides, fluorides).[40,41] When utilizing an iodide as an electrolyte, it is crucial to refer to the Pourbaix diagram, which shows the stability regions of various redox species.[42] Importantly, in the region of water stability and pH up to 7, the redox reaction (1) is favorable. Despite the reversible $I_2/2I^-$ reaction, other processes (2)–(5) can take place:[43]

$$2I^- \leftrightarrow I_2 + 2e^- \qquad (1)$$

$$I^- + I_2 \leftrightarrow I_3^- \qquad (2)$$

$$2I_3^- \leftrightarrow 3I_2 + 2e^- \qquad (3)$$

$$3I_2 + 6OH^- \leftrightarrow 5I^- + IO_3^- + 3H_2O \qquad (4)$$

$$2I_3^- + 3H_2O \leftrightarrow 5I^- + IO_3^- + 6H^+ \qquad (5)$$

A novel approach of this work is the application of the redox-active sodium iodide (NaI) as an additive into buffer solutions as an electrolyte to enhance the energy and cyclic performance of carbon-based electrochemical capacitors with stainless steel current collectors. The characteristics of the ECs were studied in acetate buffer (AcB), citrate buffer (CB), and phosphate buffer (PhB) without and with sodium iodide at different concentrations (0.2, 0.5, 1, 2 mol $L^{-1}$). The effect of various porosity commercially available activated carbons (YP50F, BP2000, YP80F) on the selected electrolytes was also taken into account. Furthermore, two additional activated carbons (Kynol, C-ST) with a high volume of micropores and larger specific surface area than YP50F were also tested. The present work reports a promising strategy to improve the performance of aqueous-based electrochemical capacitors.

## 2. Experimental section

### 2.1. Materials

Two of the buffer solutions, *i.e.*, acetic acid/sodium acetate (pH 5.12) and potassium dihydrogen phosphate/sodium hydroxide (pH 7), were provided by Fluka Analytical and used as received. Citrate buffer was prepared by mixing citric acid monohydrate and sodium hydroxide (from POCH) to obtain pH ~4. Sodium iodide ACS reagent was supplied by Sigma-Aldrich and was used for the preparation of 0.2, 0.5, 1, and 2 mol $L^{-1}$ additives for the buffer solutions. Three commercially available activated carbons were utilized as the electrode material: Black Pearl 2000 (BP2000) provided by Cabot® (USA), and YP50F and YP80F supplied by Kuraray (Japan). Additionally, carbon cloth Kynol-5092-20 was provided by Kynol company and was used as received. Moreover, highly microporous carbon was tested. This carbon (C-ST) was prepared by a salt-templated method reported elswhere.[44] Whatman GF/A (260 μm) glass fiber served as the separator. Moreover, PTFE (60% suspension in water), provided by Sigma-Aldrich, and C65 carbon black (C-NERGY™ Super C65), from Imerys, were used during the electrode preparation.

### 2.2. EC electrode preparation

The powdered activated carbons (YP50F, YP80F, C-ST) were used as the electrode materials for ECs. The electrode material consisted of 90 wt% of the selected carbon, 5 wt% of PTFE as a binder, and 5 wt% of C65 to improve the conductivity. In the case of BP2000 activated carbon, the electrode contained 85 wt% active material, 10 wt% PTFE, and 5 wt% C65. The mentioned components were mixed in the mortar, with the addition of a solvent (isopropanol) to obtain a homogenous dough-like paste. Then, the paste was press-rolled to form a thin 200 μm film in a calendaring machine. In the last step, the film was cut into disk electrodes with a diameter of 10 mm and dried for 24 h at 60 °C. Kynol electrodes were prepared by cutting carbon cloth into self-standing disks with 10 mm diameter.

### 2.3. Electrochemical characterization

The prepared electrodes were placed in symmetric two PTFE-based Swagelok® systems with stainless steel 316L current collectors. Before assembly of the device, the electrodes and separators were soaked in the selected electrolytes. The Hg/$Hg_2SO_4$ reference electrode (0.640 V *vs.* SHE) was used to monitor the potential of each electrode during the electrochemical measurements. The study of the electrochemical performance of the ECs was performed using a multi-channel potentiostat/galvanostat (VMP3, Biologic®). Cyclic voltammetry (CV) at sweep rates of 1–500 mV $s^{-1}$, galvanostatic charge/discharge (GCD) tests at current densities of 0.1–2 A $g^{-1}$, and electrochemical impedance spectroscopy (EIS) in the frequency range of 100 kHz to 1 mHz were performed for electrochemical characterization of the ECs. All the presented capacitance values of the ECs were calculated per active mass of one electrode. The long-term stability tests of the ECs were performed by the so-called floating test. The floating procedure consists of three galvanostatic charges/discharges (1 A $g^{-1}$) at a maximum operating voltage ($U_{max}$) followed by holding the voltage at $U_{max}$ for 2 h. The CV and EIS spectra were recorded after each voltage hold.

### 2.4. Physicochemical characterization

The surface area and porosity of the selected activated carbons were evaluated using Brunauer–Emmett–Teller (BET) isotherm analysis at 77 K (ASAP 2460, Micromeritics®). The pore-size distribution of the electrode materials was estimated based on the 2D non-local density functional theory (2D NLDFT). Scanning electron microscopy (SEM) observation was used to further investigate the morphology of the carbons. A conductivity meter and pH meter (both manufactured by Mettler Toledo®, Switzerland) were applied to measure the conductivity and pH of the prepared electrolytes at ambient temperature. An optical contact angle (OCA 15Pro) system equipped with a goniometer (DataPhysics®, Germany) was utilized for the wettability analysis. The SCA 20 module software, which enables the measurement of the static contact angle on a flat surface by automatically recognizing baselines and tangents,

was used for liquid droplet analysis. The injection sample volume was 8 μL and the speed was 2 μL s$^{-1}$. A PerkinElmer FTIR spectrophotometer was used to record the electrolyte absorption spectra (resolution of 4 cm$^{-1}$). A Thermo Scientific DXR-Raman microscope with a laser emitting at 532 nm and power of 5 mW was used to record the spectra in order to explain the solvent effect between the electrolytes. Powder X-ray diffraction (XRD) patterns of the different carbon materials were obtained using a Bruker D8 Advanced diffractometer operating in the Bragg–Brentano geometry with a Cu Kα radiation source ($\lambda$ = 1.5406 Å). The surface chemistry of the electrode materials was investigated by X-ray photoelectron spectroscopy (XPS) on a PHI VersaProbeII Scanning XPS system (Al Kα = 1486.6 eV) with 0.5 eV resolution and 100 μm analysis spot scanned over the area of 1600 μm$^2$.

# 3. Results and discussion

## 3.1. Electrode materials characterization

Various features of electrode materials, such as specific surface area and pore-size distribution, are important for the performance of electrochemical capacitors. Moreover, to achieve a high power and high capacitance of ECs, the ion size of the electrolyte must be smaller than the pore size of the electrode material.[18,44,45] Nitrogen adsorption/desorption isotherms and the pore-size distribution of YP50F, BP2000, and YP80F activated carbons were examined for that purpose, and the findings are shown in Fig. 1a and b. The isotherms for YP50F and YP80F activated carbons demonstrated the typical, microporous characters. However, the visible hysteresis loop at high relative pressures (0.5–0.9 $P/P_0$) suggested the presence of a small amount of mesopores, as confirmed by the volume of

mesopores equal to 0.01 cm$^3$ g$^{-1}$ for YP50F and 0.24 cm$^3$ g$^{-1}$ for YP80F (Table 1). The textural properties of the additionally tested microporous carbons (Kynol 5092-20 and C-ST) are presented in Table S1.†

Upon examining the adsorption/desorption isotherm and pore-size distribution for BP2000, it was evident that the carbon had both micropores (0.5 cm$^3$ g$^{-1}$) and mesopores (1.77 cm$^3$ g$^{-1}$). Small mesopores are essential for ECs because they act as pathways for ions that are typically solvated. It is important to match the size of ions with the pores of carbons. The diameters of the selected solvated ions, namely Na$^+$, I$^-$, HPO$_4^{2-}$, CH$_3$COO$^-$, and C$_3$H$_4$(OH)(COO)$_3^{3-}$ (Fig. 1b), were located in the region of micropores (<2 nm).[46–49] The exact values of the solvated cations diameters are presented in the ESI (Table S2†). The highest specific surface area was found for Kuraray YP80F (2018 m$^2$ g$^{-1}$), whereas YP50F and BP2000 showed lower values of 1693 and 1513 m$^2$ g$^{-1}$, respectively. The SEM image of BP2000 carbon in Fig. S1a† displayed a particle cluster structure. The SEM images of YP50F and YP80F shown in Fig. S1b and c† indicated the typical texture of activated carbons.

## 3.2. Electrolyte characterization

The electrolytic conductivity and pH of acetate, citrate, and phosphate buffers with/without 0.2 mol L$^{-1}$ NaI were measured, and the results are collected in Table 2. Overall, adding sodium iodide in various concentrations (0.2, 0.5, 1, 2 mol L$^{-1}$) increased the conductivity of all the selected buffers (Table S3†). The conductivity values for acetate buffer ranged from 63.3 to 72.2 mS cm$^{-1}$ after adding 0.2 mol L$^{-1}$ NaI. For the citrate buffer, the conductivity value changed from 3.0 to 16.5 mS cm$^{-1}$ after adding 0.2 mol L$^{-1}$ NaI. In the case of
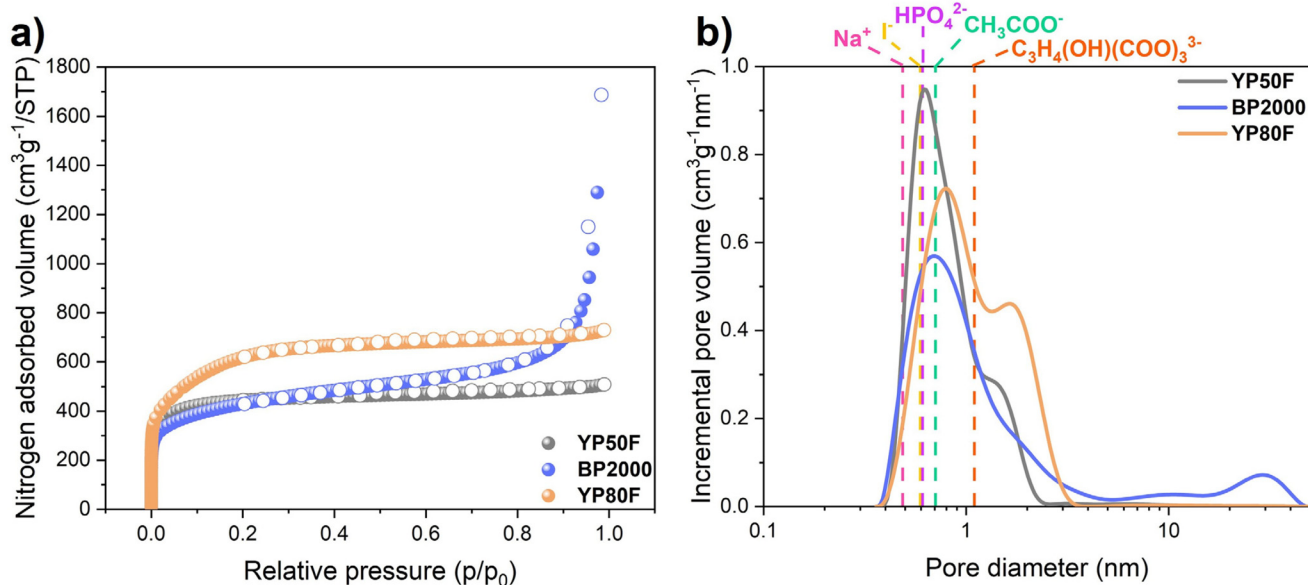


**Fig. 1** (a) Nitrogen adsorption/desorption isotherms at 77 K; (b) pore-size distributions of YP50F, BP2000, YP80F activated carbons and pore diameters of selected solvated ions.

**Table 1** Specific surface area and pore volume of the micro/mesopores of YP50F, BP2000, and YP80F activated carbons

|  | $S_{BET}$ (m$^2$ g$^{-1}$) | $V_{micro}$ (cm$^3$ g$^{-1}$) | $V_{meso}$ (cm$^3$ g$^{-1}$) |
|---|---|---|---|
| YP50F | 1693 | 0.64 | 0.01 |
| BP2000 | 1513 | 0.50 | 1.77 |
| YP80F | 2018 | 0.78 | 0.24 |

**Table 2** Conductivity (mS cm$^{-1}$) and pH values of sodium iodide (0.2 mol L$^{-1}$) and acetate buffer (AcB), citrate buffer (CB), and phosphate buffer (PhB) with/without the addition of sodium iodide (0.2 mol L$^{-1}$)

| Electrolyte | Conductivity (mS cm$^{-1}$) | pH |
|---|---|---|
| AcB | 63.3 | 5.08 |
| AcB + 0.2 mol L$^{-1}$ NaI | 72.2 | 5.05 |
| CB | 3.0 | 3.74 |
| CB + 0.2 mol L$^{-1}$ NaI | 16.5 | 3.58 |
| PhB | 6.9 | 7.18 |
| PhB + 0.2 mol L$^{-1}$ NaI | 25.5 | 6.98 |

phosphate buffer, the conductivity ranged from 6.9 to 25.5 mS cm$^{-1}$ after adding iodide. The pH values were recorded for acetate buffer (5.08), citrate buffer (3.74) and phosphate buffer (7.18) at ambient temperature. It was noted that the pH changed negligibly after the addition of selected NaI concentrations (0.2, 0.5, 1, 2 mol L$^{-1}$) into the buffers.

These results perfectly show that one of the crucial buffer features is the ability to neutralize small amounts of H$^+$ or OH$^-$ ions when they are added to solution. When the buffering capacity is surpassed, the rate of pH change rapidly increases.[50] The buffer agents were able to keep nearly the same pH after adding selected quantities of sodium iodide. FTIR and Raman spectroscopies are complementary techniques that allow evaluating the vibrational and stretching movements of different species in electrolytes. In this case, these techniques could be helpful to analyze the influence of the iodides presence on the buffer molecules stretching and vibrational modes. Here, FTIR analysis (Fig. S2a†) revealed some common features within the electrolytes, *i.e.*, the water signature associated with the O–H stretching mode with a peak centered at 3583 cm$^{-1}$, the presence of $CO_2$ diluted in each electrolyte with peak centered at 2440 cm$^{-1}$, and the presence of the C–H stretching mode associated with the peak positioned at *ca.* 600 cm$^{-1}$. After the addition of 0.2 mol L$^{-1}$ NaI to the buffer solutions, we found that the O–H stretching mode associated with the water signature positioned at 3583 cm$^{-1}$ became significantly more pronounced for the citrate and phosphate buffers, while for acetate buffer it remained the same. Signal transmittance originating from the C–H positioned at *ca.* 600 cm$^{-1}$ was significantly improved after the addition of iodides to each buffer solution due to the pronounced signal of iodides in the same frequency range of *ca.* 600 cm$^{-1}$. The Raman studies (Fig. S2b†) showed no influence from the addition of iodides on the Raman spectra. No red- or blue-shifts of the peaks were observed. The changes in the FTIR and Raman spectra were not significant. Hence, no

clear conclusions regarding the solvent effect between the buffer, iodides, and water ions could be drawn.

### 3.3. Electrochemical capacitor study

The conductivity studies showed that the addition of the smallest NaI concentration (0.2 mol L$^{-1}$) to the buffer solution significantly improved the conductivity. Owing to this, the electrochemical investigation focused mainly on the mentioned concentration. The electrochemical investigation started with the assembly of a two-electrode system utilizing YP50F electrodes, with a large specific surface area and high volume of micropores. The maximum operating voltage window of the AcB, CB, and PhB buffers with and without 0.2 mol L$^{-1}$ NaI was extended from 0.8 V to 1.8 V during the GCD technique at a 0.5 A g$^{-1}$ current density, and the results are shown in Fig. 2a, c, e (with iodides) and Fig. S3a, c, e† (without iodides). The energetic and coulombic efficiencies were calculated from GCD curves and are shown in Fig. 2b, d, f and Fig. S3b, d, f.† The coulombic efficiency, which is determined by the discharging time, was greater than 96% (at 1.5 V), indicating the best possible capacitive behavior of each EC. The energetic efficiency, calculated by integration of the discharge curve, showed values ranging from 62% for AcB + 0.2 mol L$^{-1}$ NaI, to 74% for CB + 0.2 mol L$^{-1}$ and 81% for PhB + 0.2 mol L$^{-1}$ based ECs. The GCD curves revealed a deviation above 1.5 V that was more visible in the case of AcB + 0.2 mol L$^{-1}$ NaI as well as the significant energetic efficiency drop to less than 50%. ECs based on acetate and phosphate buffers alone revealed energetic efficiencies (at 1.5 V) of 65% and 52%, respectively. Regarding the system based on citrate buffer, the energetic efficiency was significantly lower (~30%), which means that more energy was supplied during charging than recovered while discharging. The voltage extensions for the buffers with and without the iodide additive showed that all the systems were more stable with the redox pair, by showing a nearly perfect triangular shape of charge/discharge curves. Therefore, a 1.5 V limit was set as the maximum stable operating voltage for all the systems. Fig. S4† presents the voltammograms at 5 mV s$^{-1}$ for YP50F carbon-based EC operating in AcB and AcB + 0.2, 0.5, 1, 2 mol L$^{-1}$ NaI. The CV curve for AcB demonstrated a perfect rectangular shape associated with pure electrostatic attraction, which plays a crucial role in charge storage. The shape of the curves for the EC operating in AcB with NaI additives showed a deviation from a rectangular shape, as well as the rise of the specific capacitance, which was caused by the I$_2$/2I$^-$ redox activity. We also performed electrochemical studies of the voltage extension in AcB electrolyte with and without the addition of iodides by the CV method (Fig. S5†). By monitoring the electrochemical behavior of each electrode, *i.e.*, positive and negative separately (Fig. S5b†), we could observe almost square-shaped CVs resembling the behavior in standard aqueous neutral electrolytes, *e.g.*, 1 mol L$^{-1}$ Li$_2$SO$_4$.[51,52] Both electrodes had the same potential window (*i.e.*, 0.75 V) with comparable capacitance, indicating the charge-storage mechanism was based on the adsorption of ions through the formation of an electrical double-layer
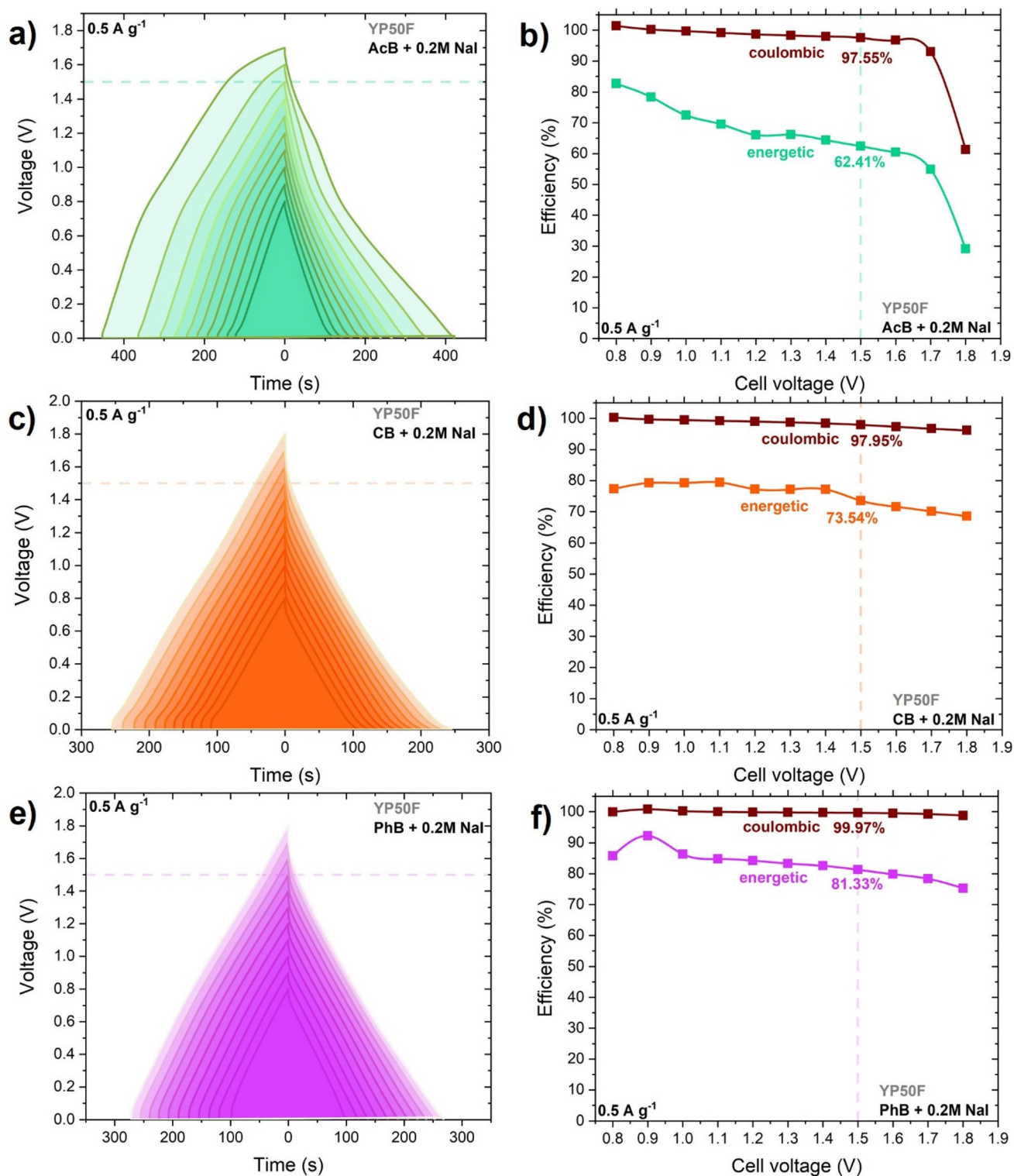
**Fig. 2** Galvanostatic charge/discharge voltage extension at 0.5 A g$^{-1}$ for ECs operating in (a) acetate buffer + 0.2 mol L$^{-1}$ NaI, (c) citrate buffer + 0.2 mol L$^{-1}$ NaI, and (e) phosphate buffer + 0.2 mol L$^{-1}$ NaI for various voltages. Energetic and coulombic efficiency calculated from the GCD curves for ECs operating in (b) acetate buffer + 0.2 mol L$^{-1}$ NaI, (d) citrate buffer + 0.2 mol L$^{-1}$ NaI, and (f) phosphate buffer + 0.2 mol L$^{-1}$ NaI.

(Fig. S5c†). After the addition of iodides to the system (AcB + 0.2 mol L$^{-1}$ NaI), the CV shape of the two-electrode cell showed small current humps, and it deviated from the ideal shape of the capacitor, indicating the strong redox activity of the iodides (Fig. S5d†). Typically, the positive electrode showed a broad and pronounced redox peak correlated with the fara-
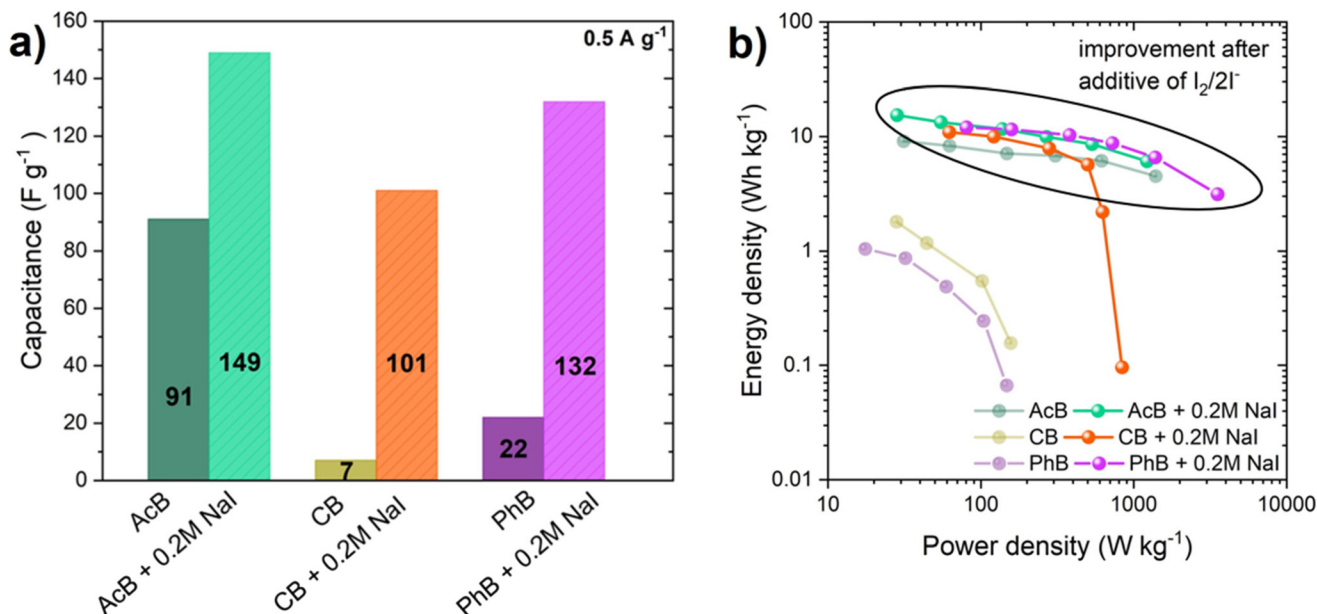
Fig. 3 (a) Specific capacitance values at 0.5 A g$^{-1}$ and (b) Ragone plots for ECs operating in acetate buffer, citrate buffer, and phosphate buffer with/without 0.2 mol L$^{-1}$ NaI additive.

daic reaction of iodides (Fig. S5e†). In comparison to the pristine buffer solution, the positive electrode in iodide showed a higher capacitance, which resulted in the unbalanced separation of charge in the system, and led to an extended potential window of the negative electrode (0.85 V) (Fig. S5f†), consequently improving the specific capacitance of the system at a high voltage window of 1.5 V. This mechanism for the iodide reaction was comparable to the other works reported on the use of iodides in electrochemical capacitors employing reactions presented by eqn (1)–(3).[53] Fig. 3a visualizes the specific capacitance values calculated from the GCD at 0.5 A g$^{-1}$ for AcB, CB, and PhB with/without 0.2 mol L$^{-1}$ NaI. The additive of the iodide/iodine redox pair enhanced the specific capacitance values for each EC, by 40% in the case of AcB, 93% for CB, and 83% for PhB. The influence of 0.2 mol L$^{-1}$ NaI additive on the energy and power metrics of the buffer-based ECs could be noticed in the Ragone plot as well (Fig. 3b).

Along with the importance of increasing the energetic characteristics of ECs, the electrochemical stability and long-time performance are also considered to be crucial factors. One of the most popular and commonly used techniques for that purpose is galvanostatic cycling. However, such a technique requires a lot of time. Therefore, a less time-consuming alternative technique (floating) was used. Floating consists of three GCD cycles with a voltage hold for 2 h at $U_{max}$. The criterion end-of-life is a 20% loss of initial capacitance or 200% increase in the initial resistance.[54] Before and after the floating tests, cyclic voltammetry at 5 mV s$^{-1}$ and electrochemical impedance spectroscopy analysis were carried out to assess the impact of the accelerated aging of ECs. The results of the floating for the different commercial carbon-based ECs

(YP50F, BP2000, and YP80F) operating in AcB with 0.2 mol L$^{-1}$ NaI and YP50F-based EC working in AcB (without iodide) are shown in Fig. S6a.† The highest long-term performance for the ECs with an iodide/iodine pair was noted for YP50F carbon (310 h) followed by 212 h for the YP80F-based EC and 126 h for the BP2000-based EC. This study revealed that carbon with a higher micropore volume presents a longer floating time than typical mesoporous ones. Presumably, the reversible I$_2$/2I$^-$ redox pair was well confined inside the micropores. Moreover, the contact angle measurements confirmed the best wettability was for YP50F. Poor wettability leads to a low utilization of the surface area, resulting in a low specific capacitance. The contact angle of 65° was measured for BP2000 carbon with acetate buffer/iodide, followed by 64° for YP80F carbon and 60° for YP50F carbon. Several concentrations of NaI additive (0.2, 0.5, 1, 2 mol L$^{-1}$) to AcB electrolyte were applied for the YP50F-based EC during the floating test (Fig. S7a†). The floating time of such systems was the best for 0.2 mol L$^{-1}$ of NaI additive (310 h), whereas for pure AcB, it was equal to 100 h only. The worst floating (34 h) was recorded for the 2 mol L$^{-1}$ NaI additive. These findings provide clear proof that the concentration of iodide additive must be carefully selected for a long lifespan of ECs. Even if a high iodide concentration supplies a high capacitance at the beginning, it does not guarantee a long cycling life, and gradually, the formed polyiodides can easily block the available surface of the carbon. The Nyquist plots before and after 100 h floating for the AcB system and 310 h floating for the AcB + 0.2 mol L$^{-1}$ NaI system are shown in Fig. S7b† and Fig. 4b, respectively.

The equivalent series resistance increased twofold in both cases, indicating the EC's end-of-life would be mainly due to
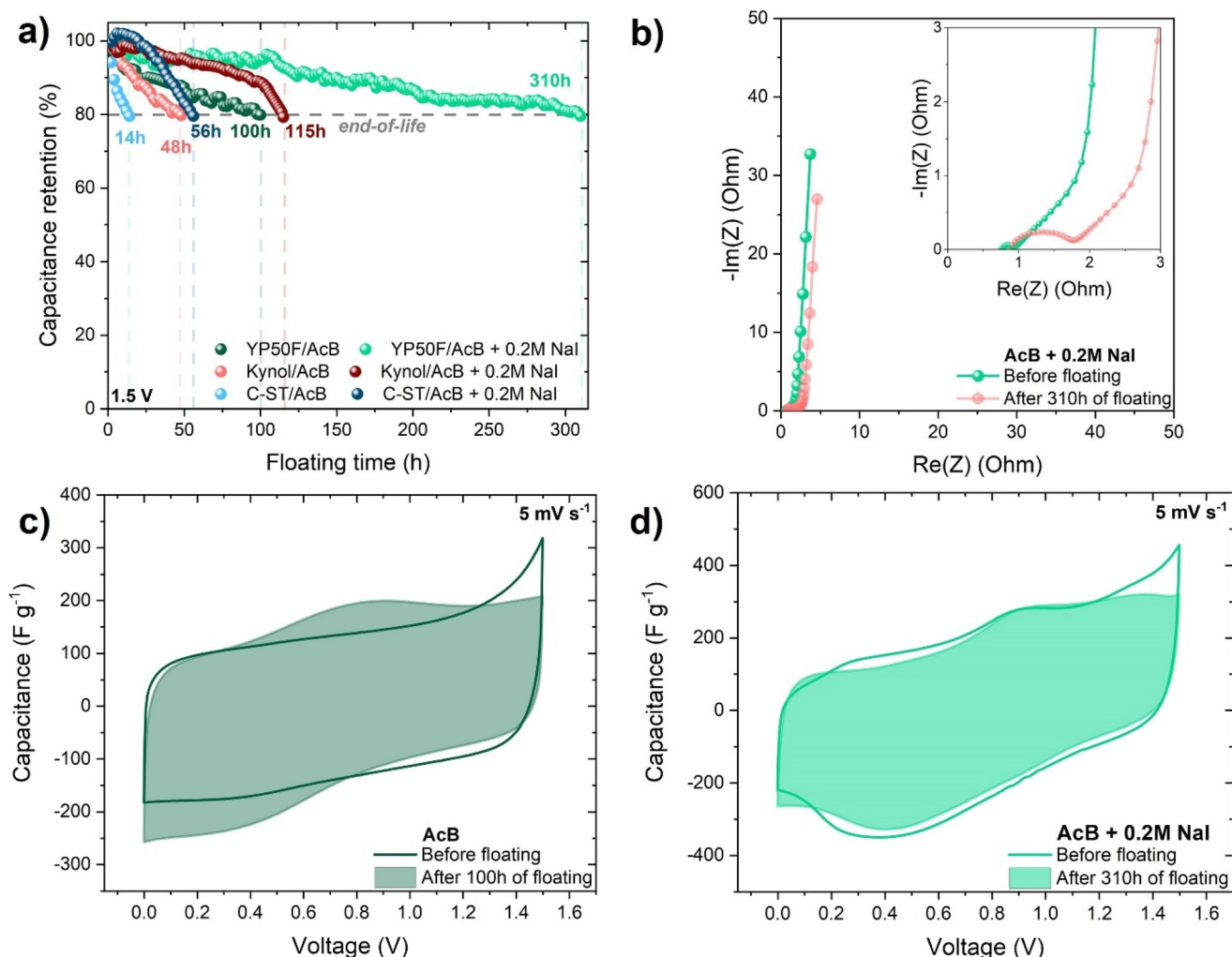
**Fig. 4** (a) Capacitance retention of different microporous carbons (YP50F, Kynol, and C-ST) based ECs operating in acetate buffer with and without 0.2 mol L$^{-1}$ NaI additive during the floating test (at 1.5 V). (b) Nyquist plots obtained from YP50F-based ECs operating in acetate buffer + 0.2 mol L$^{-1}$ NaI before and after 310 h floating test. Cyclic voltammogram at 5 mV s$^{-1}$ recorded for (c) acetate buffer before and after 100 h floating test; (d) acetate buffer + 0.2 mol L$^{-1}$ NaI before and after 310 h floating test.

the deterioration of the electrode performance (parasitic reactions) and the presence of stainless steel corrosion products. Cyclic voltammetry (5 mV s$^{-1}$) was applied in order to compare the impacts of accelerated aging for pure AcB and that with iodide additive (Fig. 4c and d). The cyclic voltammograms recorded for ECs with NaI additive after prolonged floating time exhibited almost the same charge propagation. However, they exhibited a noticeably more resistant character. Such ECs subjected to prolonged polarization at $U_{max}$ = 1.5 V were exposed to the occurrence of parasitic processes. The peaks associated with the redox activity could be attributed to the side reactions of the new functional groups on the carbon electrode surface, e.g., quinone–hydroquinone.

The electrochemical measurements proved that microporous carbon YP50F was the best choice in terms of energy density as well as long-term performance compared to the available mesoporous carbons (YP80F, BP2000). That is why, to extend the provided studies, other types of highly microporous

carbons with larger specific surface areas (Kynol, C-ST) were investigated. The galvanostatic charge/discharge technique was applied for comparison of the electrochemical performance of ECs operating in acetate buffer with and without 0.2 mol L$^{-1}$ NaI additive (Fig. S8a and b†). The development of the specific surface area to 2640 m$^2$ g$^{-1}$ as well as the micropore volume to 0.97 cm$^3$ g$^{-1}$ in the case of the salt-templated carbon (C-ST) enabled a significant increase in capacitance values for the EC operating in AcB + 0.2 mol L$^{-1}$ NaI to reach 244 F g$^{-1}$. In the case of the system based on carbon cloth (Kynol), there was also a visible increase in the capacitance value compared to the EC based on YP50F operating in acetate buffer with/without iodide additive. Both additionally tested carbons had a larger $S_{BET}$ than YP50F, which affects the electrochemical performance of ECs. Furthermore, the long-term performance of Kynol and C-ST microporous carbons operating in acetate buffer with and without I$_2$/2I$^-$ additive were analyzed (Fig. 4a). The investigation revealed that the

YP50F-based EC operating in acetate buffer + 0.2 mol L$^{-1}$ NaI, despite its lower specific surface area, showed the best long-term performance (310 h of floating), followed by 115 h of floating for the Kynol- and 56 h of floating for the C-ST-based ECs. In the ESI,† the cyclic voltammograms, Nyquist plots, and galvanostatic charge/discharge curves before and after the floating tests are provided for the YP50F-, Kynol-, and C-ST-based ECs operating in acetate buffer with/without 0.2 mol L$^{-1}$ NaI additive (Fig. S9–S11†).

After the floating tests, the electrodes were also analyzed by X-ray diffraction measurements (XRD) to study the structures of the samples and/or residues of the electrolyte components (Fig. S12†). Pristine YP50F showed broad and low intensity peaks characteristic for activated carbon positioned at *ca.* 22° and 43°, corresponding to the (002) and (100) planes of graphite structure (JCPDS 00-056-0159). Iodides underwent redox reactions on the positive electrode, effectively improving the reachable capacitance of the system, as we have shown in our manuscript. In standard aqueous electrolytes, the aging process of the electrodes included oxidation of the carbon surface eventually leading to a change of the pH at the electrode/electrolyte interface. However, the systems operating in the buffer with the iodide solutions were able to withstand such changes. Taking into account the redox activity of iodides at the positive electrode, we decided to study only (+) electrodes after floating tests operating in AcB and AcB + 0.2 mol L$^{-1}$ NaI electrolytes (Fig. S12†). It occurred that both electrodes showed broad peaks at comparable positions to the pristine YP50F. The sharp peak at *ca.* 18° corresponded to the presence of the PTFE in the electrode material. There was no presence of additional peaks, which was proof that the long-term electrochemical operation had no effect on the formation of solid-state residues, which could cause porosity blockage and deterioration of the electrochemical performance of the system.

To further study the surface chemistry of cycled electrodes, we utilized the X-ray photoelectron spectroscopy (XPS) technique. Table S4 and Fig. S13† present the surface concentrations of chemical bonds, derived from fitting the XPS data for the pristine electrode (YP50F) and electrodes (positive and negative) cycled in buffer solutions without and with the addition of sodium iodides. After the floating tests, we observed a decrease in C=C sp$^2$ bonding and an increase in C–C sp$^3$ bonding in the C 1s spectrum (Fig. S13a†) on the surface of both electrodes in comparison to the pristine YP50F electrode. This indicates that the electrochemical tests in AcB buffer electrolyte affected the surface chemistry of the electrode material, as reflected by the altered content of oxygen groups. In the case of the positive electrode, a much higher decrease in C=C sp$^2$ bonding was observed (from 56.9% to 41.4%) compared to the negative electrode (from 56.9% to 51.6%), suggesting that the positive electrode was more affected by electrochemical parasitic processes. We also observed a variation in the oxygen content in the O 1s region (Fig. S13b†). On the positive electrode, the signals from the oxygen functionalities increased, *i.e.*, in the C 1s spectrum, the signal from O–C=O at 288.9 eV increased from 3.2% to 3.8%, and in the O 1s spectrum, the signal from (C–O, –OH) at 533.8 eV increased from 2.2% to 4.9%. The content of other oxygen functionalities, such as (C–O–C, C–OH) at 286.3 eV or (–COOH) at 290.3 eV slightly decreased from 7% to 6.3% and from 2.7% to 2.2%, respectively. This suggests that after the floating tests, not all the functional groups were contributing to the increase in the oxygen content. Interestingly, we observed a comparable pattern in the case of the negative electrode (see Table S4† for details), but the changes were not as pronounced as in the case of the positive electrode.

We also investigated the surface composition of electrodes after floating in AcB + 0.2 mol L$^{-1}$ NaI electrolyte. Interestingly, the results revealed a much higher content of
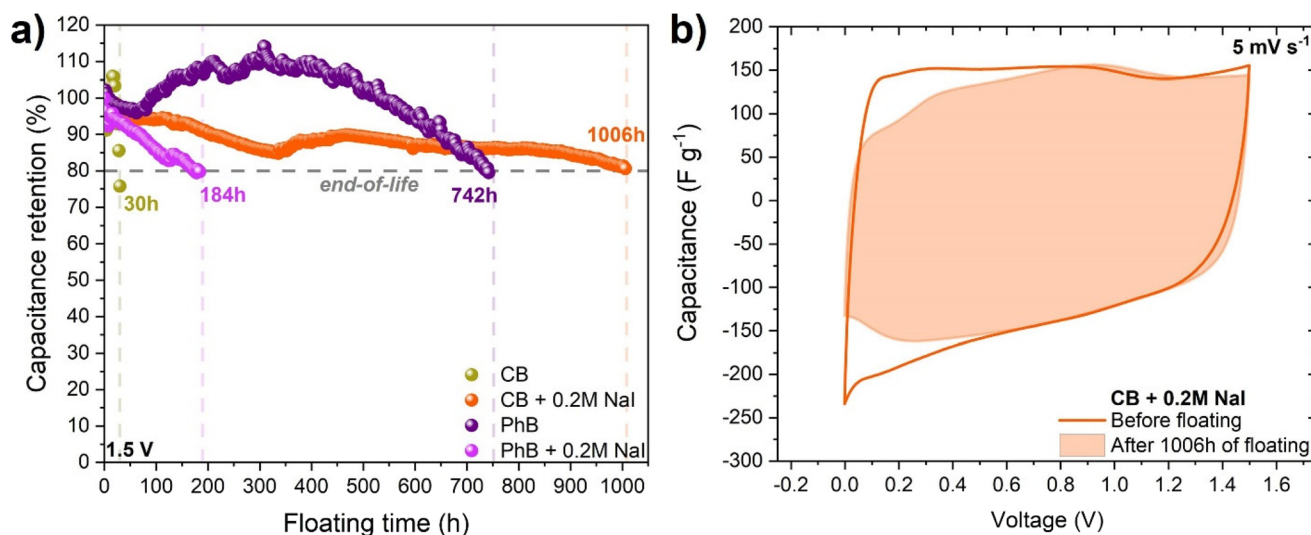


**Fig. 5** (a) Capacitance retention of YP50F-based ECs operating in citrate buffer and phosphate buffer with/without 0.2 mol L$^{-1}$ NaI additive during floating test (at 1.5 V). Cyclic voltammograms for ECs operating in (b) citrate buffer + 0.2 mol L$^{-1}$ NaI before and after 1006 h floating test.

C═C sp$^2$ bonding in comparison to the electrodes aged in AcB alone (from 56.9% to 51.2% for the negative electrode and 47.0% for the positive electrode), which could indicate that the iodides were not as oxidative as the AcB electrolyte alone. We observed a similar trend in terms of the positive electrode being more prone to oxidation, but overall, the surface of the electrodes was less oxidized than when cycled in pure AcB.

Additionally, we observed signals at 618.4 and 620.6 eV in the I 3d$_{5/2}$ spectrum (Fig. S13c†), corresponding to the presence of NaI and CH–I bonds. These provide evidence that the iodides were partly grafted on the carbon surface after the prolonged electrochemical tests. At the same time, we did not observe the presence of insolubilities in the water iodates, which suggests that the buffer solution restricted changes in the pH, preventing the electrochemical formation of side products.

Finally, the influence of 0.2 mol L$^{-1}$ NaI additive to the citrate and phosphate buffers on the ECs was tested with the floating method, as shown in Fig. 5. Surprisingly, the pure CB-based system reached only 30 h of floating. The addition of 0.2 mol L$^{-1}$ NaI into the CB-based EC significantly improved the floating time (1006 h), suggesting that the slightly acidic citrate buffer is suitable for reversible long-term iodide redox activity.

Regarding phosphate buffer-based ECs, it could be seen that some fluctuations, especially around 300 h, and a capacitance retention value above 100% took place. Such behavior was associated with not enough time for electrode soaking in the electrolyte before the experiment. The high contact angle of 70° and slower wettability time could affect the performance. Finally, the system was able to reach the end-of-life criterion after 742 h. Unexpectedly, the 0.2 mol L$^{-1}$ NaI additive to the phosphate-based EC did not improve the long-term performance, with a 184 h floating time. Such a performance could be influenced by the pH value, which was 7.18, and according to the Pourbaix diagram, it seemed to be a limit for the efficient working of the I$_2$/2I$^-$ redox pair.

## 4. Conclusions

The iodide/buffer electrolyte as an environmentally friendly and cost-effective composition was introduced for the first time for the energy enhancement of carbon-based electrochemical capacitors. The buffer environment, *i.e.*, acetate, citrate, and phosphate, with stable pH, enabled extending the operating voltage of ECs up to 1.5 V. Such a result is meaningful, since it is well-known that a stable operating voltage for iodides-based ECs is limited to 1.2 V. A noteworthy improvement of the electrochemical capacitor cycle life at a voltage of 1.5 V was achieved when 0.2 mol L$^{-1}$ NaI was added to acetate buffer and citrate buffer. During the aging test (at 1.5 V) such ECs exhibited 310 h and 1006 h prolonged floating times, respectively. These results are substantial when compared to ECs operating in pure acetate (100 h) and citrate (30 h). Moreover, the contact angle measurements of selected acti-

vated carbons with different porosities and acetate buffer + 0.2 mol L$^{-1}$ NaI revealed that highly microporous Kuraray YP50F carbon had the best wettability, as confirmed by the smallest contact angle of 60°. As a consequence, the microporous carbon-based EC operating in AcB + 0.2 mol L$^{-1}$ showed the best long-term performance (310 h) during the accelerated aging test compared to YP80F (212 h) and BP2000 (126 h) activated carbons. The galvanostatic charge/discharge carried out on ECs working in buffer electrolytes with 0.2 mol L$^{-1}$ NaI proved that such additive could significantly increase the specific capacitance values, from 91 to 149 F g$^{-1}$ for acetate buffer, from 7 to 101 F g$^{-1}$ for citrate buffer, and from 22 to 132 F g$^{-1}$ for phosphate buffer. The work evidenced that the use of a buffer as an electrolyte with iodide additive significantly improved the EC performance. The beneficial effect of the stabilized pH of such buffer-based electrolytes relies on a limited oxidation of the positive electrode. This was especially pronounced in the buffer/iodide-based electrolytes. After electrochemical floating, the covalent bonding between carbon and iodide was proven by XPS. Stabilization of the pH at the electrode/electrolyte interface prevented the formation of insoluble products. Our experiments showed negligible solvent effects for buffer/iodide-based electrolytes. Such sustainable system buffer/iodide-based electrolytes could be practically utilized. To sum up, our demonstrated buffer/iodide electrolyte-based EC is a cheap, green, and reliable approach, with significant promise for future widespread application.

## Conflicts of interest

There are no conflicts of interest to declare.

## Acknowledgements

## References

1 BP Statistical Review of World Energy (2022).
2 P. A. Owusu and S. Asumadu-Sarkodie, A review of renewable energy sources, sustainability issues and climate change mitigation, *Cogent Eng.*, 2016, **3**, 1167990.
3 G. Palmer, Renewables rise above fossil fuels, *Nat. Energy*, 2019, **4**, 538–539.
4 P. Simon, Y. Gogotsi and B. Dunn, Where do batteries end and supercapacitors begin?, *Science*, 2014, **343**, 1210–1211.
5 A. Burke, Z. Liu and H. Zhao, Present and future applications of supercapacitors in electric and hybrid vehicles, *IEEE-IEVC*, 2014, 1–8.
6 T. Shimizu and C. Underwood, Super-capacitor energy storage for micro-satellites: feasibility and potential mission applications, *Acta Astronaut.*, 2013, **85**, 138–154.
7 Y. Su, N. Li, L. Wang, R. Lin, Y. Zheng, G. Rong and M. Sawan, Stretchable transparent supercapacitors for

wearable and implantable medical devices, *Adv. Mater. Technol.*, 2022, **7**, 2100608.

8 A. Muzaffar, M. B. Ahamed, K. Deshmukh and J. Thirumalai, A review on recent advances in hybrid supercapacitors: design, fabrication and applications, *Renewable Sustainable Energy Rev.*, 2019, **101**, 123–145.

9 S. Yamazaki, T. Ito, M. Yamagata and M. Ishikawa, Non-aqueous electrochemical capacitor utilizing electrolytic redox reactions of bromide species in ionic liquid, *Electrochim. Acta*, 2012, **86**, 294–297.

10 L. Yang, L. Zhang, X. Jiao, Y. Qiu and W. Xu, The electrochemical performance of reduced graphene oxide prepared from different types of natural graphites, *RSC Adv.*, 2021, **7**, 4042–4052.

11 I. Piñeiro-Prado, D. Salinas-Torres, R. Ruiz-Rosas, E. Morallón and D. Cazorla-Amorós, Design of activated carbon/activated carbon asymmetric capacitors, *Front. Mater.*, 2016, **3**, 16.

12 J. Chmiola, G. Yushin, R. K. Dash, E. N. Hoffman, J. E. Fischer, M. W. Barsoum and Y. Gogotsi, Double-layer capacitance of carbide derived carbons in sulfuric acid, *Electrochem. Solid-State Lett.*, 2005, **8**, A357.

13 A. Halder, M. Ghosh, M. A. Khayum, S. Bera, M. Addicoat, S. H. Sasmal, S. Karak, S. Kurungot and R. Banerjee, Interlayer hydrogen-bonded covalent organic frameworks as high-performance supercapacitors, *J. Am. Chem. Soc.*, 2018, **35**, 10941–10945.

14 H. Furukawa, K. E. Cordova, M. O'Keeffe and O. M. Yaghi, The chemistry and applications of metal-organic frameworks, *Science*, 2013, **341**, 1230444.

15 B. Anasori, M. R. Lukatskaya and Y. Gogotsi, 2D metal carbides and nitrides (MXenes) for energy storage, *Nat. Rev. Mater.*, 2017, **2**, 1–17.

16 C. Niu, E. K. Sichel, R. Hoch, D. Moy and H. Tennent, High power electrochemical capacitors based on carbon nanotube electrodes, *Appl. Phys. Lett.*, 1997, **70**, 1480–1482.

17 M. Fu, W. Chen, Y. Lei, H. Yu, Y. Lin and M. Terrones, Biomimetic construction of ferrite quantum dot/graphene heterostructure for enhancing ion/charge transfer in supercapacitors, *Adv. Mater.*, 2023, **35**, 2300940.

18 K. Zou, P. Cai, B. Wang, C. Liu, J. Li, T. Qiu, G. Zou, H. Hou and X. Ji, Insights into enhanced capacitive behavior of carbon cathode for lithium ion capacitors: the coupling of pore size and graphitization engineering, *Nano-Micro Lett.*, 2020, **12**, 121.

19 A. Balducci, Electrolytes for high voltage electrochemical double layer capacitors: a perspective article, *J. Power Sources*, 2016, **326**, 534–540.

20 V. Khomenko, E. Raymundo-Piñero, E. Frackowiak and F. Béguin, High-voltage asymmetric supercapacitors operating in aqueous electrolyte, *J. Appl. Phys. A*, 2006, **82**, 567–573.

21 L. Suo, O. Borodin, T. Gao, M. Olguin, J. Ho, X. Fan, C. Luo, C. Wang and K. Xu, Water-in-salt electrolyte enables high-voltage aqueous lithium-ion chemistries, *Science*, 2015, **350**, 938–943.

22 S. E. M. Pourhosseini, A. Bothe, A. Balducci, F. Beguin and P. Ratajczak, Strategy to assess the carbon electrode modifications associated with the high voltage ageing of electrochemical capacitors in organic electrolyte, *Energy Storage Mater.*, 2021, **38**, 17–29.

23 A. Balducci, U. Bardi, S. Caporali, M. Mastragostino and F. Soavi, Ionic liquids for hybrid supercapacitors, *Electrochem. Commun.*, 2004, **6**, 566–570.

24 W. Zaidi, A. Boisset, J. Jacquemin, L. Timperman and M. Anouti, Deep eutectic solvents based on N-methylacetamide and a lithium salt as electrolytes at elevated temperature for activated carbon-based supercapacitors, *J. Phys. Chem. C*, 2014, **118**, 4033–4042.

25 S. Azmi, A. Klimek and E. Frackowiak, Anticorrosive performance of green deep eutectic solvent for electrochemical capacitor, *Chem. Eng. J.*, 2022, **444**, 136594.

26 S. Azmi, A. Klimek and E. Frackowiak, Why electrochemical capacitor electrolytes should not be ignored?, *Electrochim. Acta*, 2023, **452**, 142347.

27 C. Li, W. Wu, P. Wang, W. Zhou, J. Wang, Y. Chen, L. Fu, Y. Zhu, Y. Wu and W. Huang, Fabricating an aqueous symmetric supercapacitor with a stable high working voltage of 2 V by using an alkaline–acidic electrolyte, *Adv. Sci.*, 2019, **6**, 1801665.

28 K. Fic, G. Lota, M. Meller and E. Frackowiak, Novel insight into neutral medium as electrolyte for high-voltage supercapacitors, *Energy Environ. Sci.*, 2012, **2**, 5842–5850.

29 A. Slesinski, S. Sroka, K. Fic, E. Frackowiak and J. Menzel, Operando monitoring of local pH value changes at the carbon electrode surface in neutral sulfate-based aqueous electrochemical capacitors, *ACS Appl. Mater. Interfaces*, 2022, **33**, 37782–37792.

30 C. H. Chien, T.-H. Wu, M. Rajkumar and C.-C. Hu, Effects of buffer agents on hydrogen adsorption and desorption at/within activated carbon for the negative electrode of aqueous asymmetric supercapacitors, *Electrochim. Acta*, 2016, **205**, 1–7.

31 S. T. Vindt and E. M. Skou, The buffer effect in neutral electrolyte supercapacitors, *Appl. Phys. A*, 2016, **122**, 64.

32 E. Proksch, Buffering capacity, *Curr. Probl. Dermatol.*, 2018, **54**, 11–18.

33 H. Hashiba, L.-C. Weng, Y. Chen, H. K. Sato, S. Yotsuhashi, C. Xiang and A. Z. Weber, Effects of electrolyte buffer capacity on surface reactant species and the reaction rate of $CO_2$ in electrochemical $CO_2$ reduction, *J. Phys. Chem. C*, 2018, **7**, 3719–3726.

34 R. A. Durst, *Standard reference materials: standardization of pH measurements*, U.S. Department of Commerce, Rogers C. B. Morton, 1975.

35 A. Salis and M. Monduzzi, Not only pH. Specific buffer effects in biological systems, *Curr. Opin. Colloid Interface*, 2016, **23**, 1–9.

36 B. Wang, Q. Fan, L. Xu, J. Liu, C. Dai, M. Tang, K. Liang, P. L. Taberna, Y. Liu, P. Simon and Z. Lin, Activating pseudocapacitive charge storage of molten-salt-synthesized

MXenes in mild aqueous electrolytes, *ACS Appl. Energy Mater.*, 2023, DOI: 10.1021/acsaem.3c02376.

37  S. Makino, T. Ban and W. Sugimoto, Towards implantable bio-supercapacitors: pseudocapacitance of ruthenium oxide nanoparticles and nanosheets in acids, buffered solutions, and bioelectrolytes, *J. Electrochem. Soc.*, 2015, **162**, A5001.

38  J. Piwek, A. Platek, K. Fic and E. Frackowiak, Carbon-based electrochemical capacitors with acetate aqueous electrolytes, *Electrochim. Acta*, 2016, **215**, 179–186.

39  S. Zallouz, L. Dentzer and C. Matei Ghimbeu, Carbon capacitors operating at 1.8 V based on concentrated aqueous electrolytes: impacts of the electrolyte concentration and carbon properties, *ACS Appl. Energy Mater.*, 2024, **7**, 1448–1460.

40  G. Lota and E. Frackowiak, Striking capacitance of carbon/iodide interface, *Electrochem. Commun.*, 2009, **11**, 87–90.

41  S. E. Chun, B. Evanko, X. Wang, D. Vonlanthen, X. Ji, G. D. Stucky and S. W. Boettcher, Design of aqueous redox-enhanced electrochemical capacitors with high specific energies and slow self-discharge, *Nat. Commun.*, 2015, **6**, 7818.

42  A. Platek-Mielczarek, E. Frackowiak and K. Fic, Specific carbon/iodide interactions in electrochemical capacitors monitored by EQCM technique, *Energy Environ. Sci.*, 2021, **4**, 2381–2393.

43  A. Platek, J. Piwek, K. Fic and E. Frackowiak, Ageing mechanisms in electrochemical capacitors with aqueous redox-active electrolytes, *Electrochim. Acta*, 2019, **311**, 211–220.

44  A. Platek-Mielczarek, C. Nita, C. Matei Ghimbeu, E. Frackowiak and K. Fic, Link between alkali metals in salt templates and in electrolytes for improved carbon-based electrochemical capacitors, *ACS Appl. Mater. Interfaces*, 2021, **13**, 2584–2599.

45  B. Yan, J. Zheng, L. Feng, Q. Zhang, C. Zhang, Y. Ding, J. Han, S. Jiang and S. He, Pore engineering: structure-capacitance correlations for biomass-derived porous carbon materials, *Mater. Des.*, 2023, **229**, 111904.

46  I. Persson, Hydrated metal ions in aqueous solution: how regular are their structures?, *Pure Appl. Chem.*, 2010, **82**, 1901–1917.

47  B. Tansel, Significance of thermodynamic and physical characteristics on permeation of ions during membrane separation: hydrated radius, hydration free energy and viscous effects, *Sep. Purif. Technol.*, 2012, **86**, 119–126.

48  M. V. Fedotova and S. E. Kruchinin, Hydratation of acetic acid and acetate ion in water studied by 1D-RISM theory, *J. Mol. Liq.*, 2011, **164**, 201–206.

49  D. Moreno, Y. Bootwala, W.-Y. Tsai, Q. Gao, F. Shen, N. Balke, K. B. Hatzell and M. C. Hatzell, In situ electrochemical dilatometry of phosphate anion electrosorption, *Environ. Sci. Technol.*, 2018, **5**, 745–749.

50  V. Chiriac and G. Balea, Buffer index and buffer capacity for a simple buffer solution, *J. Chem. Educ.*, 1997, **8**, 937.

51  K. Fic, A. Platek, J. Piwek, J. Menzel, A. Slesinski, P. Bujewska, P. Galek and E. Frackowiak, Revisited insights into charge storage mechanisms in electrochemical capacitors with Li$_2$SO$_4$-based electrolyte, *Energy Storage Mater.*, 2019, **22**, 1–14.

52  J. Menzel, A. Slesinski, P. Galek, P. Bujewska, A. Kachmar, E. Frackowiak, A. Washio, H. Yamamoto, M. Ishikawa and K. Fic, Operando monitoring of activated carbon electrodes operating with aqueous electrolytes, *Energy Storage Mater.*, 2022, **49**, 518–528.

53  G. Lota, K. Fic and E. Frackowiak, Alkali metal iodide/carbon interface as a source of pseudocapacitane, *Electrochem. Commun.*, 2011, **13**, 38–41.

54  P. Ratajczak, K. Jurewicz, P. Skowron, Q. Abbas and F. Béguin, Effect of accelerated ageing on the performance of high voltage carbon/carbon electrochemical capacitors in salt aqueous electrolyte, *Electrochim. Acta*, 2014, **130**, 344–350.